Time-domain measurement of terahertz frequency magnetoplasmon resonances in a two-dimensional electron system by the direct injection of picosecond pulsed currents

Jingbo Wu,[1] Oleksiy Sydoruk,[2] Alexander S. Mayorov,[1] Christopher D. Wood,[1] Divyang Mistry,[1] Lianhe Li,[1] Edmund H. Linfield,[1] A. Giles Davies,[1] and John E. Cunningham[1,a)]

[1]*School of Electronic and Electrical Engineering, University of Leeds, Woodhouse Lane, Leeds LS2 9JT, United Kingdom*

[2]*Optical and Semiconductor Devices Group, Department of Electrical and Electronic Engineering, Imperial College London, South Kensington Campus, London SW7 2AZ, United Kingdom*

(Received 12 December 2015; accepted 21 February 2016; published online 3 March 2016)

We have investigated terahertz (THz) frequency magnetoplasmon resonances in a two-dimensional electron system through the direct injection of picosecond duration current pulses. The evolution of the time-domain signals was measured as a function of magnetic field, and the results were found to be in agreement with calculations using a mode-matching approach for four modes observed in the frequency range above 0.1 THz. This introduces a generic technique suitable for sampling ultrafast carrier dynamics in low-dimensional semiconductor nanostructures at THz frequencies.

[http://dx.doi.org/10.1063/1.4943173]

Mesoscopic structures fabricated from laterally patterned two-dimensional electron systems (2DESs) often have energy gaps in the meV range resulting from quantum confinement, and as such, their resulting energy spectrum is accessible using terahertz (THz) frequency spectroscopy. At the same time, picosecond timescale time-domain measurements of mesoscopic systems are of fundamental interest since they offer a means to study time-resolved carrier dynamics. However, because the dimensions of mesoscopic systems are typically much smaller than the wavelength of free-space propagating THz radiation, efficient coupling between the two is challenging.

Early studies at GHz frequencies of magnetoplasmons in 2DESs (plasmon excitations of the carriers, coupled to cyclotron resonances driven by a magnetic field) used direct current injection to provide access to magnetic field-induced spectra,[1–5] with Muravev *et al.*[6] recently demonstrating a low-frequency (up to ∼few GHz) relativistic magnetoplasmon mode. THz measurements, on the other hand, have typically relied on grating couplers,[7–10] metamaterials[11,12] or capacitive coupling between a lossy on-chip THz waveguide in proximity to a 2DES.[13,14] Unfortunately, while grating couplers and metamaterials can be used to convert incident THz radiation that is out-of-plane with the 2DES to in-plane, they are not appropriate for probing THz response of individual subwavelength samples. In contrast, whilst capacitive coupling allows the magnetoplasmon spectra of an individual 2DES mesa to be recovered, it is difficult to remove the background signal which does not pass through 2DES, since only a portion of the signal couples into the 2DES from the waveguide, and is therefore influenced by it, with the remainder propagating in the waveguide. Furthermore, it is somewhat difficult to establish the geometric boundary of the THz excitation, since it is the gap between the center conductor and the ground planes in a coplanar waveguide (CPW) that provides coupling to the 2DES.

In this letter, we show that the concept of direct current injection commonly used at GHz frequencies can be extended to the THz frequency range, allowing both a straightforward analysis of magnetoplasmon spectra, and direct comparison with theory. We use a technique whereby a 2DES is probed using few-picosecond current pulses obtained by exciting, with a femtosecond laser, monolithically integrated low-temperature-grown GaAs (LT-GaAs) photoconductive (PC) switches, which are connected to the 2DES by a coplanar waveguide.[15,16] The current pulses not only directly excite cavity plasmon modes in the 2DES but are also used to measure the formation, and evolution, of 2D magnetoplasmon modes dynamically in a magnetic field.

A schematic diagram of the device and wafer structure is shown in Figs. 1(a) and 1(b), respectively. A 73–μm-long GaAs/AlGaAs heterostructure mesa which contains a 2DES at the interface of a GaAs buffer and an AlGaAs layer was incorporated into a CPW. Two pairs of LT-GaAs PC switches (S1/S2 and S3/S4) formed on either side of the 2DES mesa were used to generate (by application of a bias voltage between the probe arm and the center conductor of the CPW) or to detect few-picosecond-duration current pulses upon illumination by a 100 fs pulse duration Ti:sapphire laser. A 4.4-μm-long metallic gate was overlaid across the 2DES mesa, and a negative bias was used both to control the carrier concentration underneath the gate and to provide modulation, as discussed later. The carrier concentration (n_s) and mobility (μ) of the unbiased 2DES mesa were obtained at 1.4 K from magnetoresistance measurements of a Hall bar fabricated from the same wafer. The n_s

a)Electronic email: j.e.cunningham@leeds.ac.uk

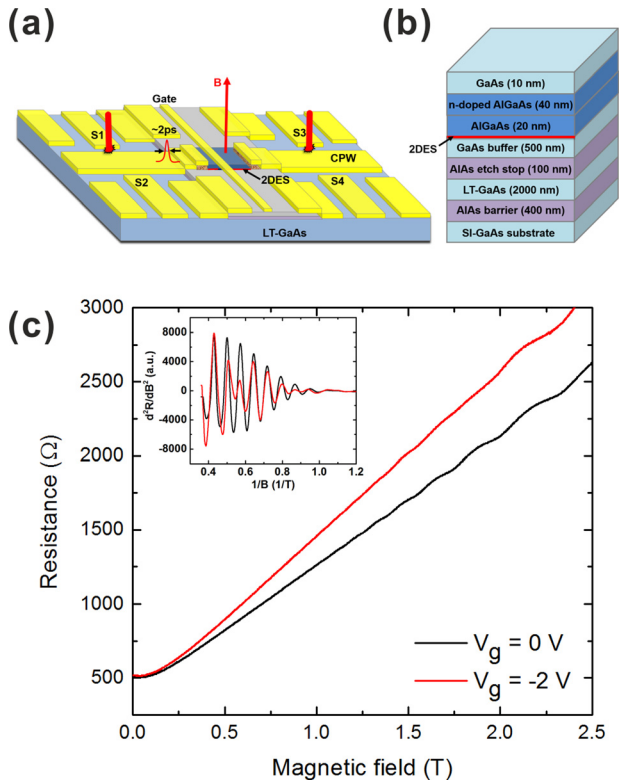

FIG. 1. (a) Schematic diagram showing the THz circuit in which a 2DES mesa is integrated with an on-chip THz time-domain spectrometer. S1/S2 and S3/S4 are two pairs of photoconductive switches used to generate and detect the THz pulses. The magnetic field is applied perpendicular to the 2DES plane. (b) The layer structure of the wafer used for device fabrication. (c) The resistance of the 2DES mesa (R) as a function of magnetic field (B) when $V_g = 0$ V (black) and -2 V (red) at 2 K. Inset: the second derivative of R with respect to B (d^2R/dB^2) plotted as a function of $1/B$.

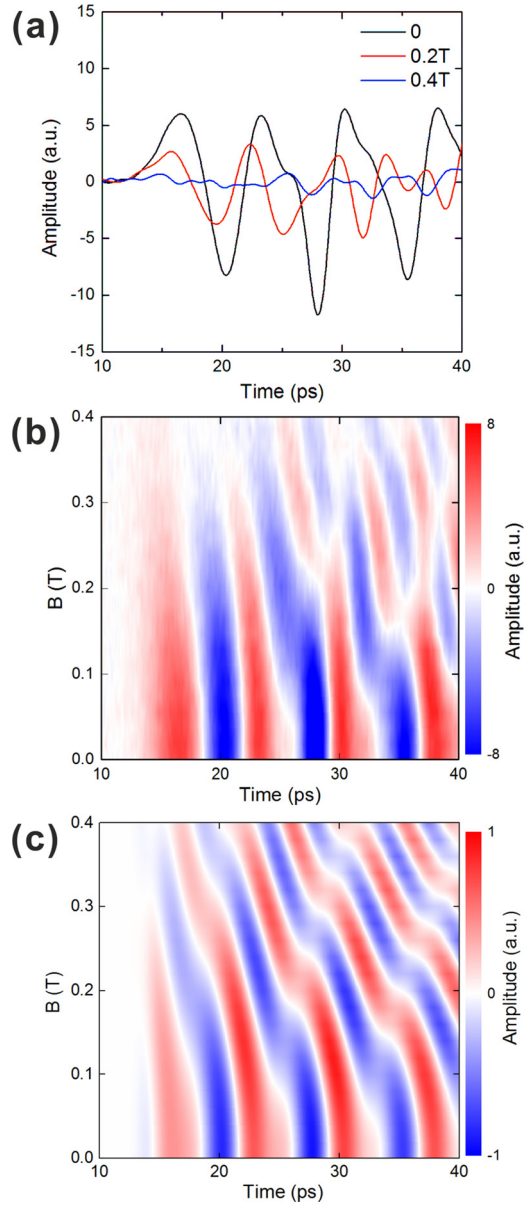

FIG. 2. (a) The gate-modulation signal as a function of time delay measured at $V_g = -2.0$ V and for $B = 0$, 0.2, and 0.4 T. (b) Color-scale plot of the experimentally measured gate-modulation signals as a function of time delay and magnetic field at 2 K. (c) Simulated time-domain profiles of gate-modulation signals in (b).

obtained from the measured Hall coefficient was $6.3 \times 10^{11}\,\mathrm{cm}^{-2}$, and μ was found to be $9.0 \times 10^5\ \mathrm{cm}^2/(\mathrm{V\,s})$ from the diagonal resistance at 0 T. Our complete device (Fig. 1(a)) was mounted onto a sample holder attached to the mixing plate of a cryogen-free dilution refrigerator, and positioned at the center of a superconducting magnet.[16] As shown in Fig. 1(a), a magnetic field was applied normal to the 2DES plane. The device fabrication procedure and the experimental arrangement in the dilution refrigerator were similar to those described in Ref. 15.

Figure 1(c) shows the two-terminal DC resistance of the 2DES mesa measured as a function of magnetic field for gate voltage (V_g) of 0 V and -2 V at 2 K. The resistance of the 2D leads, connecting wires and center conductor of CPW were not subtracted. The two-terminal resistance contains contributions from the diagonal and transverse components of resistance,[17] so that at high magnetic fields, quantum Hall plateau was observed.[18] By calculating the second derivative of the resistance with respect to the magnetic field (d^2R/dB^2), weak oscillations periodic in the reciprocal of magnetic field ($1/B$) for $V_g = 0$ V were resolved (inset in Fig. 1(c)), resulting from Shubnikov-de Haas oscillations.[18,19] Their period ($\Delta(1/B)$) of $13.55\,\mathrm{T}^{-1}$ was obtained from a fast Fourier transform (FFT) spectrum of d^2R/dB^2. Using the relationship $\Delta(1/B) = 2e/n_s h$, where e is the elementary charge and h is Planck's constant, the carrier concentration n_s was calculated to be $6.5 \times 10^{11}\,\mathrm{cm}^{-2}$. For $V_g = -2$ V, the difference of n_s between the gated and ungated regions results in two oscillations of different periods. Correspondingly, the n_s in the gated and ungated regions are calculated to be 4.9×10^{11} cm^2 and 6.5×10^{11} cm^2, respectively.

If a magnetic field is applied perpendicular to a 2DES, charge carriers in the 2DES are subject to the Lorentz force, and therefore perform cyclotron motion, with a cyclotron resonance frequency given by $f_c = eB/2\pi m^*$, where m^* is the effective electron mass. For GaAs 2DES, $m^* = 0.067\ m_0$, where m_0 is the electron rest mass.[18] Coupling between the plasmon and cyclotron resonances, however, leads to a modified magnetoplasmon spectrum. In the electrostatic approximation and assuming a single resonator, a 2D magnetoplasmon frequency (f_{mp}) can be shown to satisfy the condition,

$$f_{mp}^2 = f_p^2 + f_c^2, \tag{1}$$

where f_p is the plasmon frequency at a zero magnetic field.[7,20] As discussed below, however, rigorous numerical calculations that take into account retardation and resonator coupling confirm the validity of Eq. (1) for our system.

To probe the magnetoplasmons in the 2DES channel at THz frequencies, time-domain signals were measured for a series of incremented magnetic fields. A THz pulse was generated by pulsed excitation (from a 100 fs Ti:sapphire laser) of PC switch S1, which was biased by a DC voltage of 15 V. This pulse was confined to a CPW before being injected into the 2DES mesa through an ohmic contact. The signal transmitted through the 2DES was then detected at PC switch S3, which was excited by a time-delayed portion of the same laser beam incident on S1. Similar signals were obtained using excitation of switch S2 with detection at S4. A gate-modulation technique was used to improve the signal-to-noise ratio,[15] using an AC voltage of 25 mV rms at 87 Hz as the reference.

In Fig. 2(a), the measured gate-modulation signals for $V_g = -2.0$ V both with and without magnetic field are plotted as a function of the time delay between the input (S1) and output (S3) switches. In zero field, periodic oscillations are observed, consistent with our earlier measurements,[15] which after an FFT were found to result mainly from two dominant resonance peaks centered at 130 GHz and 260 GHz, corresponding to the fundamental and second-order plasmon resonances of the gated cavity. The oscillations were weaker at $B = 0.2$ T than at $B = 0$ T, disappearing completely when B reached 0.4 T.

The decrease in the amplitude of oscillation is mainly attributed to the increase in the resistance of 2DES mesa with the increasing magnetic field, as shown in Fig. 1(c), which causes the increasing impedance mismatch to the coplanar waveguide. Meanwhile, the maxima and minima of the oscillations were both found to shift to shorter times as the magnetic field increased, indicating that the resonance frequency evolves with magnetic field.

To characterize the evolution of the oscillating signals with magnetic field, we measured the gated-modulation signals from 0 to 0.4 T with a step size of 0.02 T. The signal at $V_g = -2$ V is shown in Fig. 2(b). As the magnetic field was increased, the oscillations moved to shorter times, in accordance with Eq. (1).

To simulate the time-domain signals obtained in magnetic field, we modelled the behaviour of the two strongest resonances at different magnetic fields using the measured signal at 0 T and Eq. (1). We obtained the individual time-domain signals of the two modes by applying band-pass filters to the measured gate-modulation signal at $V_g = -2$ V and $B = 0$ T in Fig. 2(a). The filters were centered at the predicted resonant frequencies, and each had a bandwidth of 80 GHz. We note that the sum of these two signals resembles the shape of the original signal very closely, implying that these two modes make the largest contribution to the overall measured signal. We then calculated the phase φ_1 of each plasmon mode, as a function of time t using a wave approximation,

$$\varphi_1(t, V_g) = \omega_g(V_g)t + \varphi_0(V_g), \tag{2}$$

where ω_g is the angular frequency of the gated plasmon mode and φ_0 is a reference phase. Since the measured gate-modulation signal is a differential one, we used a simple model to calculate the time-domain signal of a single mode in which the loss in the gated region is taken into account. For example, we take the measured signal ($\Delta I(t,V_g)$) to be the difference between two sinusoidal waves

$$\Delta I(t,V_g) \approx A\left(\sin\varphi_1(t,V_g+V_{mod}) - \sin\varphi_1(t,V_g-V_{mod})\right)e^{-\frac{(t-t_0)}{\tau}}, \tag{3}$$

where A is the amplitude, τ is the decay time, and t_0 is the reference time. A gradient method was used to search for the best parameters of A, φ_0, and τ to fit the experimental data. The extracted τ for the fundamental and second gated mode is 17 ± 0.5 and 15 ± 1.5 ps, respectively. In the following, the magnetoplasmon frequencies of the two different modes over a range of B from 0 T to 0.4 T were calculated using Eq. (1) and the corresponding plasmon mode frequency at $B = 0$ T. Substituting the calculated magnetoplasmon frequencies and the extracted parameters (A, φ_0, and τ) of the fundamental and second modes into Eq. (3), we obtained time-domain signals of these two modes as a function of magnetic field. By summing the two signals, we simulated time-domain profiles for a range of magnetic fields from 0 T to 0.4 T (Fig. 2(c)). The amplitude of the oscillations in Fig. 2(c) remains the same when magnetic field is increased from 0 T to 0.4 T. This is because the decrease of the plasmonic oscillation amplitude with increasing magnetic field was not taken into account. Despite this, the magnetic field dependence of the measured time-domain signals is well reproduced by this approach.

We notice that there are several transitions from a single-peak to double-peak structure in both Figs. 2(b) and 2(c). Since the gate-modulation signals comprise the combination of the signals from two plasmon modes, the oscillation peak will be enhanced if the modes are in phase. Otherwise the oscillation peak will split into two. As the magnetic field is increased, both mode frequencies blue-shift continuously, resulting in a change in the phase difference between the two modes.

Fig. 3 shows the FFT of the experimental data in Fig. 2(b). There are two main resonance peaks, corresponding to the fundamental and excited (second) mode of the gated plasmon cavity. In addition, there are several relatively weak resonances, which we attribute, as discussed below, to either resonances in the two ungated cavities, or coupled resonances in the gated and neighbouring ungated cavities.[15,21] With increasing magnetic field, all of these modes blue-shift.

The ungated and gated 2DES regions in our device form a system of three coupled resonators, to which we apply a magnetic field. To simulate the modes of this system in greater detail, we calculated the frequency of hybridized resonances as a function of magnetic field using the mode-matching technique developed in Refs. 21 and 22. Maxwell's equations were first solved separately in an infinitely long gated and ungated 2DES to obtain the eigenmode spectra, which contain both plasmons and non-plasmonic modes. The effects of the magnetic field are included by

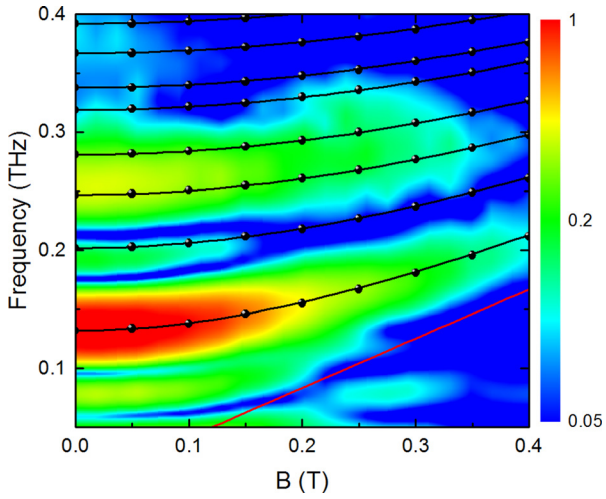

FIG. 3. Color-scale plot of the FFT amplitude spectra of the gate-modulation signals from Fig. 2(b). The black circles are the theoretical resonance frequencies calculated using a mode-matching technique, and the solid black lines are theoretical predictions from a simple quadratic law. The red line is the calculated cyclotron resonance frequency.

taking the Lorenz force on the electrons into account and replacing ω^2 with $\omega^2 - \omega_c^2$ in the equations for a 2DES but not for the dielectrics. Here, ω is the angular frequency of a wave and ω_c is the angular cyclotron frequency. The electric and magnetic fields in the three resonators were then presented as a superposition of these eigenmodes, and the fields at the junctions between the gated and ungated 2DES resonators were matched using standard Maxwell boundary conditions; the ohmic contacts were treated as perfect reflectors. A set of plasmonic transmission and reflection coefficients were obtained, which formed transmission matrices for all three 2DES cavities, from which the resonant frequencies for varying magnetic fields were calculated.

In Fig. 3, the theoretical resonant frequencies as a function of magnetic field (black circles) are shown, overlaid on an FFT color-scale plot of the experimental data. Also, shown by solid lines are the resonance frequencies obtained by the theoretical values at zero magnetic field in Eq. (1). As can be seen, the results of the full numerical calculations follow perfectly the simple law. Eight resonance modes are predicted in total. The agreement between the theory and experiments is good for the four lowest theoretical modes, although we note that the fourth mode only manifests itself as a shoulder on the (broader) third mode in the experimental data. The two strongest modes (starting at around 0.13 and 0.25 THz at $B = 0$ T) correspond to modes of the gated cavity. There is also evidence of higher modes (beyond the fourth mode) in the measured signals at low magnetic fields, although correspondence with the calculations for higher modes becomes progressively weaker. We also note that we did not find a theoretical resonance mode corresponding to the weak lowest mode measured at ~80 GHz. Indeed, no uncoupled 2D plasmonic resonance should theoretically exist at such a low frequency. We speculate that this mode may have a different, possibly polaritonic origin,[6] not accounted for by our simulations. We also note that our theoretical approach takes into account coupling between 2DES solely by plasmons, and thus ignores the possibility of a direct coupling between the two ungated cavities. Such coupling could take place at lower frequencies, where the width of the gated region (4.4 μm) is relatively small.

In conclusion, the evolution of THz frequency range 2D magnetoplasmon resonances were measured as a function of magnetic field in the time-domain using picosecond-duration pulse injection from monolithically integrated regions of a photoconductive semiconductor. The experimentally measured resonance frequencies were found to be in good agreement with a theory based on mode matching. Noting that a wide variety of low-dimensional structures can be fabricated from a 2DES, our work provides a generic methodology for the study of ultrafast dynamics in mesoscopic semiconductor systems at THz frequencies.

This work was supported by the Engineering and Physical Sciences Research Council [EP/F029543/1]. Funding was also received from the European Community's Seventh Framework Programme [FP7-IDEAS-ERC] under Grant Agreement No. 247375 "TOSCA." Support from the Royal Society and Wolfson Foundation is also acknowledged. All data supporting this study are freely available at http://dx.doi.org/10.5518/23.

[1]R. C. Ashoori, H. L. Stormer, L. N. Pfeiffer, K. W. Baldwin, and K. West, Phys. Rev. B **45**, 3894 (1992).
[2]N. B. Zhitenev, R. J. Haug, K. V. Klitzing, and K. Eberl, Phys. Rev. B **49**, 7809 (1994).
[3]G. Ernst, R. J. Haug, J. Kuhl, K. V. von Klitzing, and K. Eberl, Phys. Rev. Lett. **77**, 4245 (1996).
[4]N. Kumada, H. Kamata, and T. Fujisawa, Phys. Rev. B **84**, 045314 (2011).
[5]N. Kumada, S. Tanabe, H. Hibino, H. Kamata, M. Hashisaka, K. Muraki, and T. Fujisawa, Nat. Commun. **4**, 1363 (2013).
[6]V. M. Muravev, P. A. Gusikhin, I. V. Andreev, and I. V. Kukushkin, Phys. Rev. Lett. **114**, 106805 (2015).
[7]T. N. Theis, J. P. Kotthaus, and P. J. Stiles, Solid State Commun. **24**, 273 (1977).
[8]E. Batke, D. Heitmann, and C. W. Tu, Phys. Rev. B **34**, 6951 (1986).
[9]K. Nogajewski, J. Łusakowski, W. Knap, V. V. Popov, F. Teppe, S. L. Rumyantsev, and M. S. Shur, Appl. Phys. Lett. **99**, 213501 (2011).
[10]I. Grigelionis, K. Nogajewski, G. Karczewski, T. Wojtowicz, M. Czapkiewicz, J. Wróbel, H. Boukari, H. Mariette, and J. Łusakowski, Phys. Rev. B **91**, 075424 (2015).
[11]G. Scalari, C. Maissen, C., Turčinková, D., Hagenmüller, S. De Liberato, C. Ciuti, C. Reichl, D. Schuh, W. Wegscheider, M. Beck, and J. Faist, Science **335**, 1323–1326 (2012).
[12]C. Maissen, G. Scalari, F. Valmorra, M. Beck, J. Faist, S. Cibella, R. Leoni, C. Reichl, C. Charpentier, and W. Wegscheider, Phys. Rev. B **90**, 205309 (2014).
[13]E. A. Shaner and S. A. Lyon, Phys. Rev. B **66**, 041402(R) (2002).
[14]E. A. Shaner, S. A. Lyon, and L. W. Engel, Proc. SPIE **5352**, 364–371 (2004).
[15]J. Wu, A. S. Mayorov, C. D. Wood, D. Mistry, L. Li, W. Muchenje, M. C. Rosamond, L. Chen, E. H. Linfield, A. G. Davies, and J. E. Cunningham, Sci. Rep. **5**, 15420 (2015).
[16]C. D. Wood, D. Mistry, L. H. Li, J. E. Cunningham, E. H. Linfield, and A. G. Davies, Rev. Sci. Instrum. **84**, 085101 (2013).
[17]T. G. Powell, C. C. Dean, and M. Pepper, J. Phys. C: Solid State Phys. **17**, L359 (1984).
[18]J. H. Davies, *The Physics of Low-Dimensional Semiconductors: An Introduction* (Cambridge University Press, Cambridge, 1998).
[19]C. S. Chang, H. Fetterman, and C. R. Viswanathan, J. Appl. Phys. **66**, 928 (1989).
[20]K. W. Chiu and J. J. Quinn, Phys. Rev. B **9**, 4724 (1974).
[21]O. Sydoruk, J. B. Wu, A. Mayorov, C. D. Wood, D. M. Mistry, and J. Cunningham, Phys. Rev. B **92**, 195304 (2015).
[22]O. Sydoruk, K. Choonee, and G. C. Dyer, IEEE Trans. Terahertz Sci. Technol. **5**, 486–496 (2015).